Photo-electrochemical hydrogen production from neutral phosphate buffer and seawater using micro-structured p-Si photoelectrodes functionalized by solution-based methods

Anurag Kawde[1,2], *Alagappan Annamalai*[3], *Lucia Amidani*[2], *Manuel Boniolo*[4], *Wai Ling Kwong*[4], *Anita Sellstedt*[5], *Pieter Glatzel*[2], *Thomas Wågberg*[3], *Johannes Messinger*[1,4*]

[1] Umeå University, Department of Chemistry, Sweden

[2] European Synchrotron Radiation Facility (ESRF), Grenoble, France

[3] Umea University, Department of Physics, Sweden

[4] Molecular Biomimetics, Department of Chemistry - Ångström Laboratory, Uppsala University, Sweden

[5] Umeå University, Department of Plant Physiology, Umeå Plant Science Centre (UPSC), Umeå, Sweden

[*] Corresponding author. E-mail address: *johannes.messinger@kemi.uu.se*

Experimental section:

Synthesis, functionalization and fabrication of p-Si photoelectrode

High aspect ratio, single crystal p-Si photoelectrodes were synthesized by electroless chemical etching using $AgNO_3$, HF and H_2O_2, according to Peng et al.[1]. All the chemicals were purchased from Sigma Aldrich unless otherwise specified. The experimental steps involved in the synthesis of p-Si photoelectrodes are shown schematically in Figure 1 (main manuscript). The etched Si obtained after step-2 is referred to as 'as-synthesized' p-Si in the following. As the experiments involve the use of corrosive and toxic chemicals like HF, piranha and HNO_3 solutions, the experiments were performed within a fume-hood and using recommended protective gear.

The as-synthesized p-Si were first spin-coated with TiO_2 sol and subsequently the co-catalysts CoO_x, or NiO_x were applied in a similar way using their sols. The TiO_2 sol was prepared by vigorous mixing of Titanium (IV) butoxide (TIB, Ti-$(OCH_2CH_2CH_2CH_3)$4, 2-butanol, HCl (35.5%) and pluronic P-123 (a triblock copolymer) in the molar ratio 1:2:0.0139:9. A well-mixed TiO_2 sol then was spin-coated onto the as-synthesized p-Si substrates ($2cm^2$) at 4000 rpm in three cycles followed by annealing at 380 °C for two hours. The NiO_x sol was prepared by dropwise addition of isopropanol into a stirred 0.5 M nickel acetate tetra hydrate ($Ni(OCOCH_3)_2 \cdot 4H_2O$) solution in ethylene glycol to yield the final ratio of 2:3 (v/v) isopropanol in Ni-solution. The CoO_x sol was prepared in a similar way by adding dropwise 0.1 M nitric acid to a stirred solution of 0.5 M of $Co(NO_3)_2 \cdot 6H_2O$ (99.999% on metal basis) in deionized (DI) water to yield the final ratio of 0.3 : 49.7 (v/v). The precursor solution was spin-coated in nine steps (1 ml each; 30 seconds each at 4000 rpm) onto the p-Si/TiO_2 , which was followed by annealing at 380 °C for two hours in order to obtain p-Si/TiO_2/NiO_x and p-Si/TiO_2/CoO_x photoelectrodes, respectively.

Morphological, Photo-electrochemical and X-ray Spectroscopic measurements

As synthesized and functionalized p-Si were examined by scanning electron microscopy (SEM), energy dispersive X-ray (EDX) and X-Ray photoelectron spectroscopy (XPS) to study their morphology and elemental composition.

Photo-electrochemistry

Prior to photoelectrochemical experiments, all edges of the photoelectrodes were first polished with sand paper. The top edge of the electrode was attached to a crocodile clip and this assembly was sealed with conductive silver paste. The remaining three edges were instead coated with insulting epoxy. A gas-tight three-electrode quartz cell from Pine Instruments, Durham-USA, equipped with a Ag/AgCl reference electrode and a platinum counter electrode (OER), was used to measure the photo-electrochemical HER-electrode properties of the functionalized p-Si using a solar simulator (Newport- 94043A, equipped with 450W Xenon lamp and air-mass 1.5 filter) and a potentiostat (Metrohm Autrolab PGSTAT302N). The photo-electrochemical results reported here were obtained at 1 sun (100 mW/cm^2) illumination in an aqueous 0.1 M phosphate buffer (pH 7.0) or artificial seawater (pH 8.4). The artificial seawater (pH 8.4) was prepared by dissolving 23.476 g NaCl, 4.981 g $MgCl_2$, 3.917 g Na_2SO_4, 1.102 g $CaCl_2$, 0.664 g KCl, 0.192 g $NaHCO_3$, 0.096 g KBr, 0.026 g H_3BO_3, 0.024 g $SrCl_2$ and 0.003 g NaF in 1 litre deionized water.[2]

Linear sweep voltammetry (LSV) and electrochemical impendence spectroscopy (EIS) were performed in the dark and under one-sun illumination to record the photocurrent response of the functionalized p-Si. LSVs were performed vs. Ag/AgCl with a sweep rate of 10 mV/s without iR compensation. The (EIS) measurements were performed using an impedance analyzer (Autolab PGSTAT302N with FRA module). The impedance spectra were measured over a frequency range of 0.01 Hz to 1 MHz at 25 °C with an amplitude of 10 mV and under an applied potential of -0.6 V vs. Ag/AgCl and one sun illumination. The Mott-Schottky plots were derived from impedance measurement in the dark at 10 kHz.

For measuring the Faradaic efficiency, the gas-tight PEC cell was purged with argon for 3 hours to remove dissolved oxygen from the electrolyte and from the headspace. The amounts of molecular hydrogen and oxygen produced by photo-electrochemical water splitting at 0.0 VRHE under one sun illumination were measured by taking, at various times, 100 µl aliquots from the headspace using a gas tight syringe. These headspace aliquots were then analyzed at room temperature by gas chromatography using a GC-8AIT gas chromatograph with a TCD detector (Schimadzu Scientific Instruments, Columbia, USA).[3]

The applied bias photon to current conversion efficiency (ABPE) was calculated using Equation S1.

$$ABPE = \frac{(|j\ (mA\ cm^{-2}|) \times \left(1.23 - |V_b|\right)(V)\ \times\ FE}{P_{sun}\ (mWcm^{-2})}$$

Eq. S1

Where, *j* is the photocurrent density, V_b is the potential versus ideal counter electrode, FE is the Faradaic efficiency and P_{sun} is the incident solar power at AM 1.5 G (100 mW/cm^2).

The Faradaic efficiency (FE) was calculated using Equation S2.

$$FE = \frac{Amount\ of\ hydrogen\ generated}{Amount\ of\ hydrogen\ expected} \times 100$$

Eq. S2

The theoretical H_2 production was calculated using Equation S3.

$$Q(mol\ of\ H_2) = \frac{(|j|) \times t}{n\ \times F}$$

Eq. S3

where, *j* is the photocurrent density in mA normalized to illuminated photoelectrode surface area, t is the time in seconds, n is the number of electron transferred during HER ($2e^-$) and F is the Faraday constant 96485.3 s A mol^{-1}.

The carrier concentration was calculated from the slopes of the Mott-Schottky plots using the equation S4.

$$N_D = \left(\frac{2}{e^0 \varepsilon \varepsilon^0}\right) / \left(\frac{d(\frac{1}{C^2})}{dV}\right) \qquad \textbf{Eq.S4}$$

where, e0 is the electron charge, ε is the dielectric constant of Si, ε0 is the vacuum permittivity, ND is the carrier density, C is the capacitance between the sample and the electrolyte and V is the applied bias across the photoelectrode during the Mott-Schottky measurements.

X-ray spectroscopy

The X-ray absorption and emission spectroscopy (XAS-XES) was carried out on beamline ID-26 of the European Synchrotron radiation facility. A schematic view of the optics and the experimental set up is presented elsewhere.[4, 5] The high-energy resolution fluorescence detected X-ray absorption near edge structure (HERFD-XANES) and emission spectroscopies were performed at the Ti K-α fluorescence line. A Si <111> double crystal monochromator was used to tune the incident beam at the Ti K-edge energy. A Ti foil was used to calibrate the incident X-ray energy. The size of the X-ray beam on the sample was 0.7 mm in horizontal and 0.2 mm in vertical. Higher harmonics were suppressed by total external reflection using three Si mirrors at 2.5 mrad. The high-energy resolution fluorescence detected X-ray absorption near edge structure (HERFD-XANES) spectra were recorded at the maximum of the Ti Kα_1 line. The fluorescence energy was selected by five Ge <400> bent crystal analyser arranged in Rowland geometry.[4, 6] The X-ray photons selected by the crystal analysers were focused on an avalanche photodiode. The samples were placed into a fluorescence geometry, where the incident beam and the central crystal analyser were at 45^0 with respect to the normal to the sample surface and a 90^0 angle between the incident beam and the central crystal analyser. All HERFD-XANES and Kα XES spectra reported here were normalized with respect to the total area. Fluorescence-detected absorption spectra show spectral distortions because of incident beam self-absorption or over-absorption effects. One consequence of self-absorption is an increased pre-edge spectral intensity. No attempt was made to correct for this but we compare in Figures 7 and ESI Figure S9 only spectra with similar self-absorption. The conclusions we draw here are not affected by this spectral distortion.

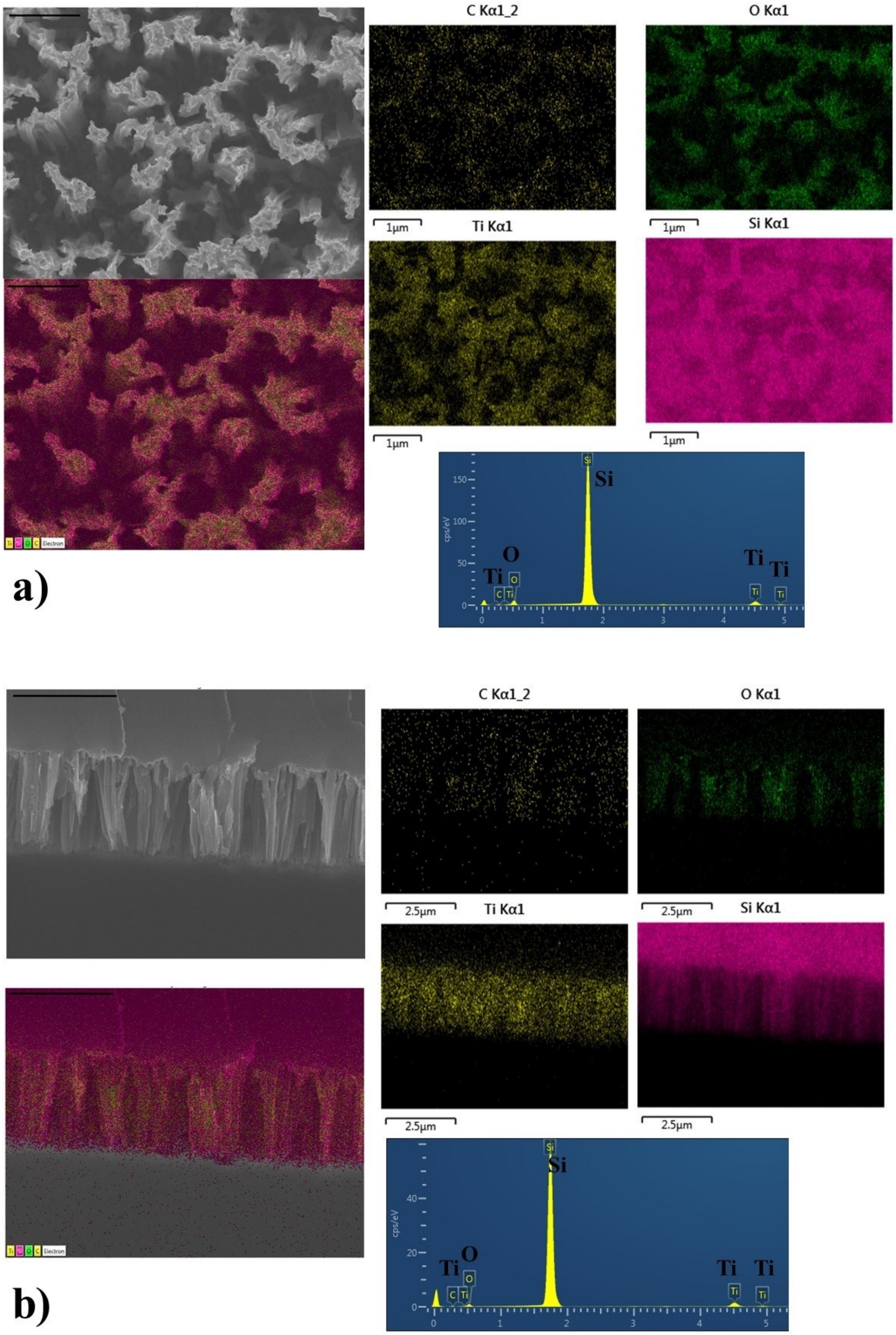

Figure S1: SEM EDX mapping of p-Si/TiO_2: **(a)** Planar and **(b)** cross-sectional

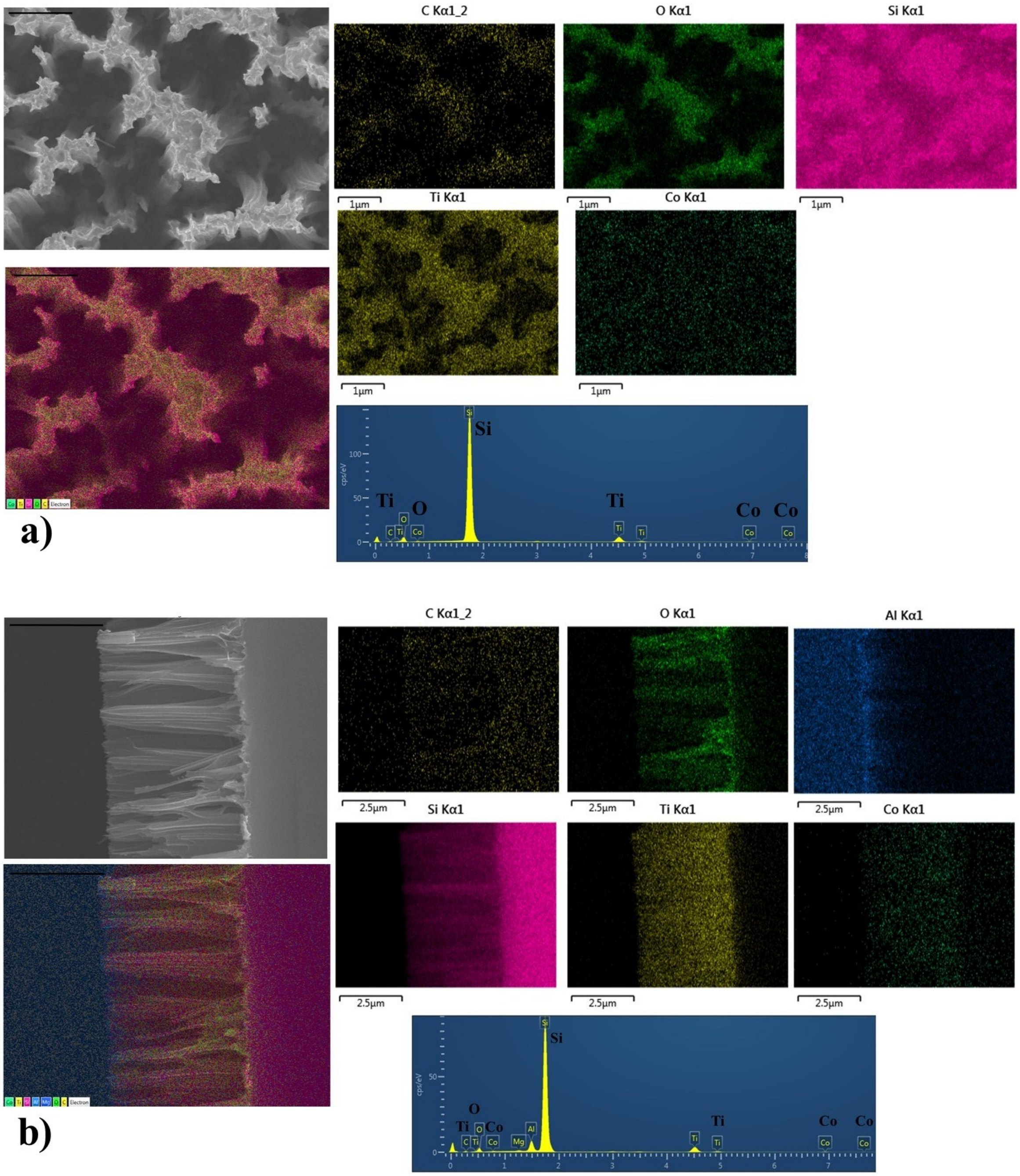

Figure S2: SEM EDX mapping of p-Si/TiO_2/CoO_x: **(a)** Planar and (**b)** cross-sectional

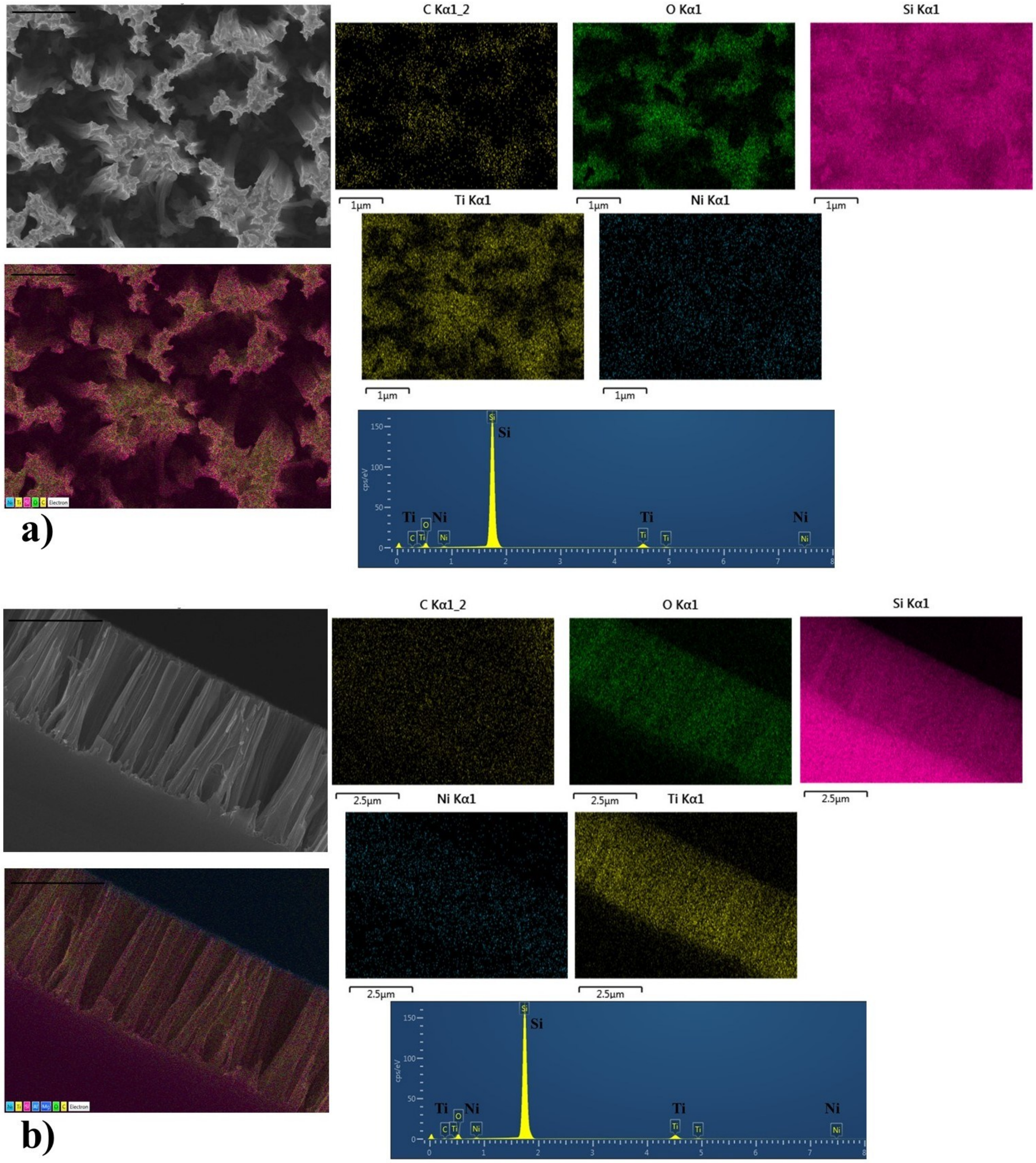

Figure S3: SEM EDX mapping of p-Si/TiO_2/NiO_x: **(a)** Planar and (**b)** cross-sectional

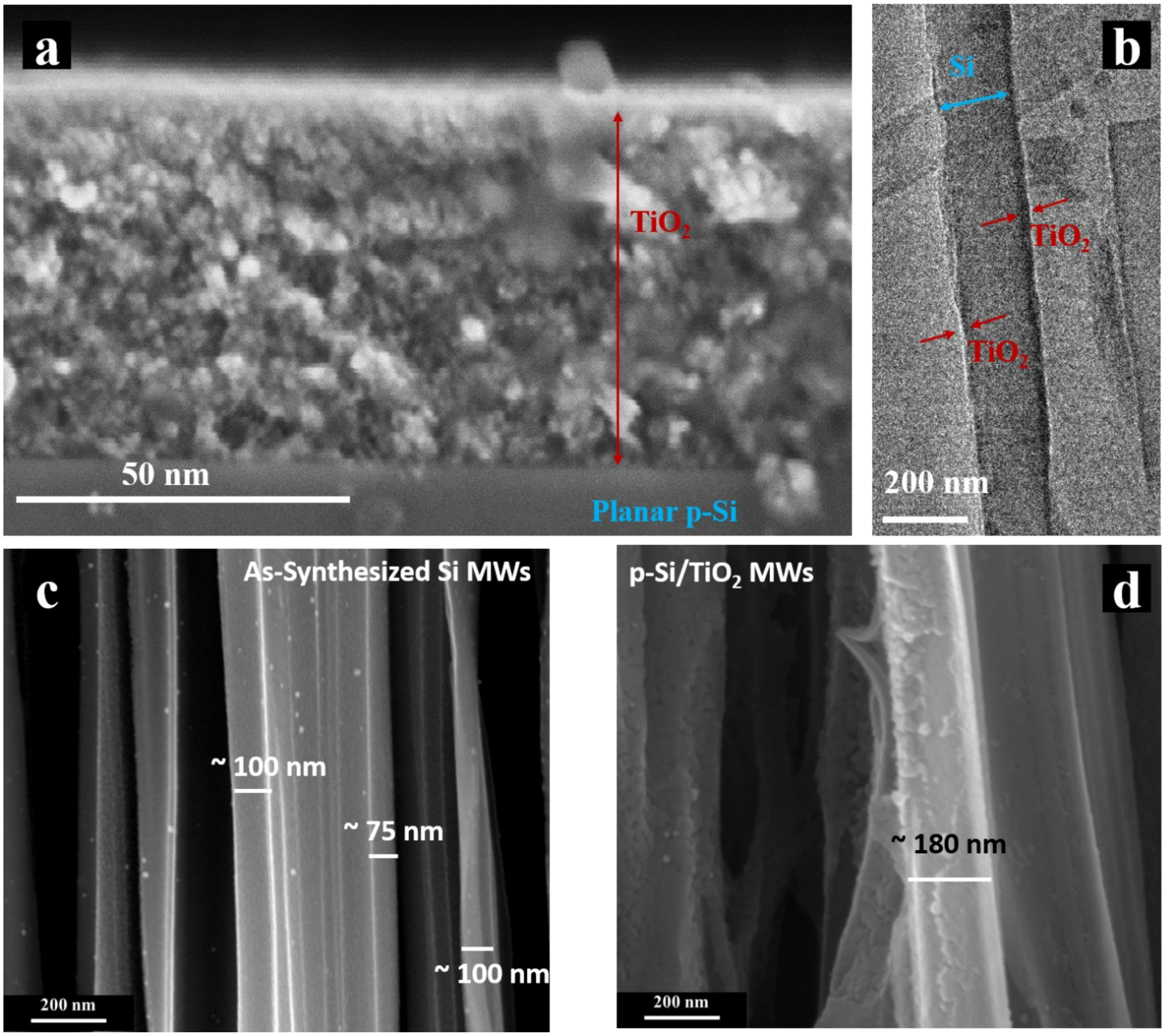

Figure S4: (a) SEM image of planar p-Si coated with TiO_2 and (b) TEM image of a p-Si microwire coated with a TiO_2 layer of thickness between about 20 nm. (c) SEM image of uncoated p-Si microwires, and (d) SEM image of a TiO_2 coated Si microwire. The comparison of (c) and (d) leads to a thickness estimate for the TiO_2 layer of 40-50 nm.

Explanation of size estimate: Figure S4 (a) shows the thickness of TiO_2 achieved by spin coating of planar p-Si to be ~ 50 nm. It is more difficult to determine the thickness of TiO_2 on the surface of p-Si microwire (MW) from SEM images. Panels c shows that the thickness of the uncoated MW varies typically between about 75-100 nm, but the full range is about 50-200 nm. Since the TiO_2 layer often connects neighboring MW, it is not easy to get a similar statistics for TiO_2-coated Si MW. Panel d shows one example that has an overall diameter of about 180 nm. Assuming that a 'typical' Si MW is under this coating, one may estimate the thickness of the TiO_2 layer to 40-50 nm.

For obtaining independent information that allows distinguishing between Si and TiO_2, we performed TEM to determine the thickness and uniformity of TiO_2 on the surface of p-Si microwire. Figure S4 (b) shows a TEM image of an individual p-Si/TiO_2 microwire indicating the thickness of TiO_2 in between about 20 nm.

As we do not have good statistics on this, and because MW with the thinner coating may detach preferentially from the support during the TEM sample preparation procedure, we conservatively estimate the thickness of the TiO_2 layer to be between 20-50 nm.

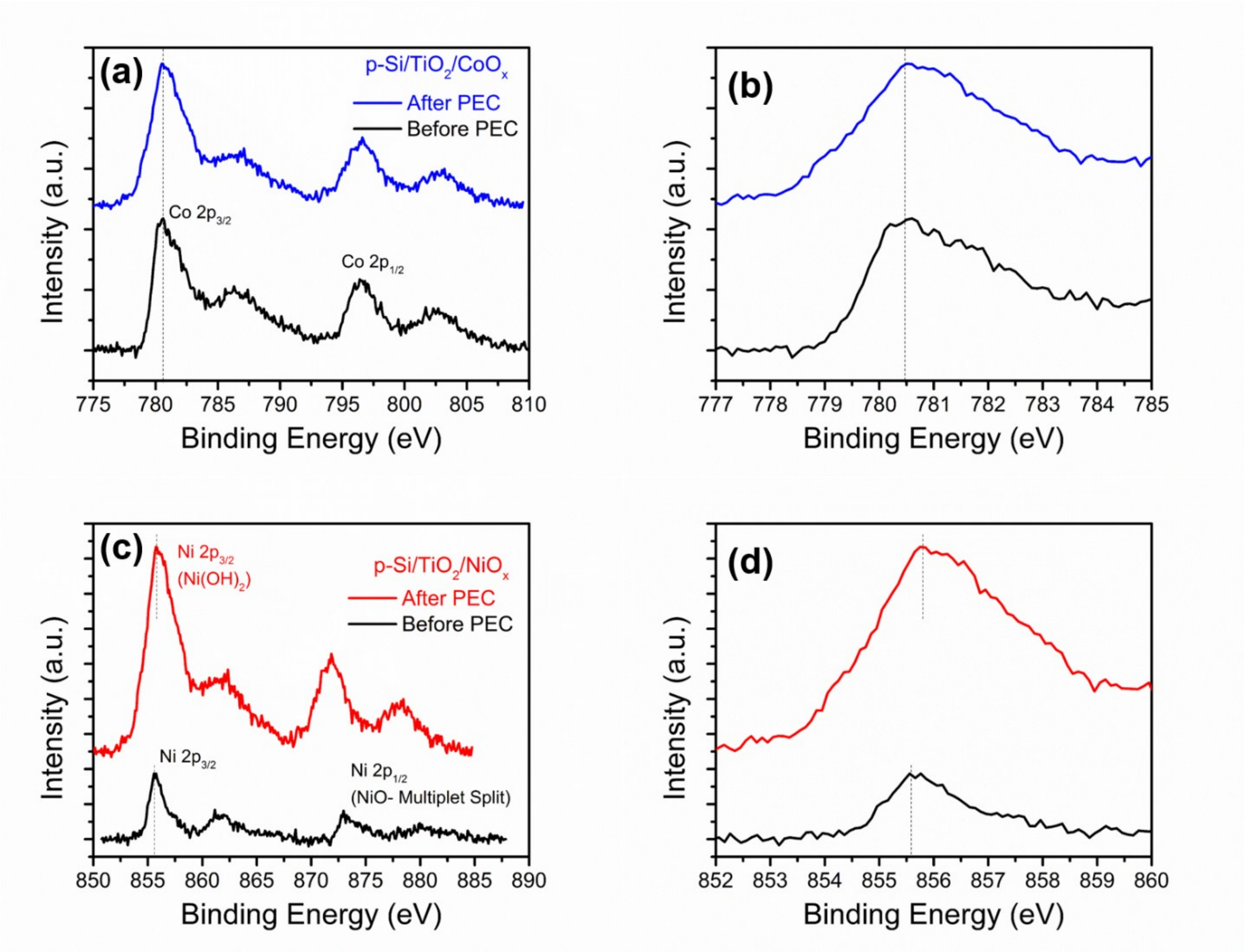

Figure S5: XPS spectra of p-Si/TiO_2/CoO_x and p-Si/TiO_2/NiO_x photoelectrodes before and after PEC experiment: **(a)** The Co 2p photoelectron emission spectrum reveals two intense satellite peaks at~ 786.4 eV and ~ 802.7 eV, consistent with the presence of Co^{2+} as CoO_x.[7, 8] The CoO_x samples do not appear to change during the PEC experiment as no shift was observed in the Co $2p_{3/2}$ peaks. Additionally, a peak at BEs ~782.5 (Co $2p_{3/2}$) confirms presence of Co as Co^{2+} oxide. **(c)** The NiO_x samples before the PEC experiment shows two intense satellite peaks at~ 879.9 eV and ~ 861.8 eV and additional peaks at ~873 eV (Ni $2p_{1/2}$) and ~855.5 eV (Ni $2p_{3/2}$) suggesting the presence of Ni^{2+} in a mixture of NiO_x and $Ni(OH)_2$.[9, 10] The shift in Ni $2p_{3/2}$ peak to binding energy ~ 855.7 after the PEC experiment suggest an increased percentage of $Ni(OH)_2$. **(b and d)** are the enlarged views of Co and Ni $2p_{3/2}$ peaks respectively.

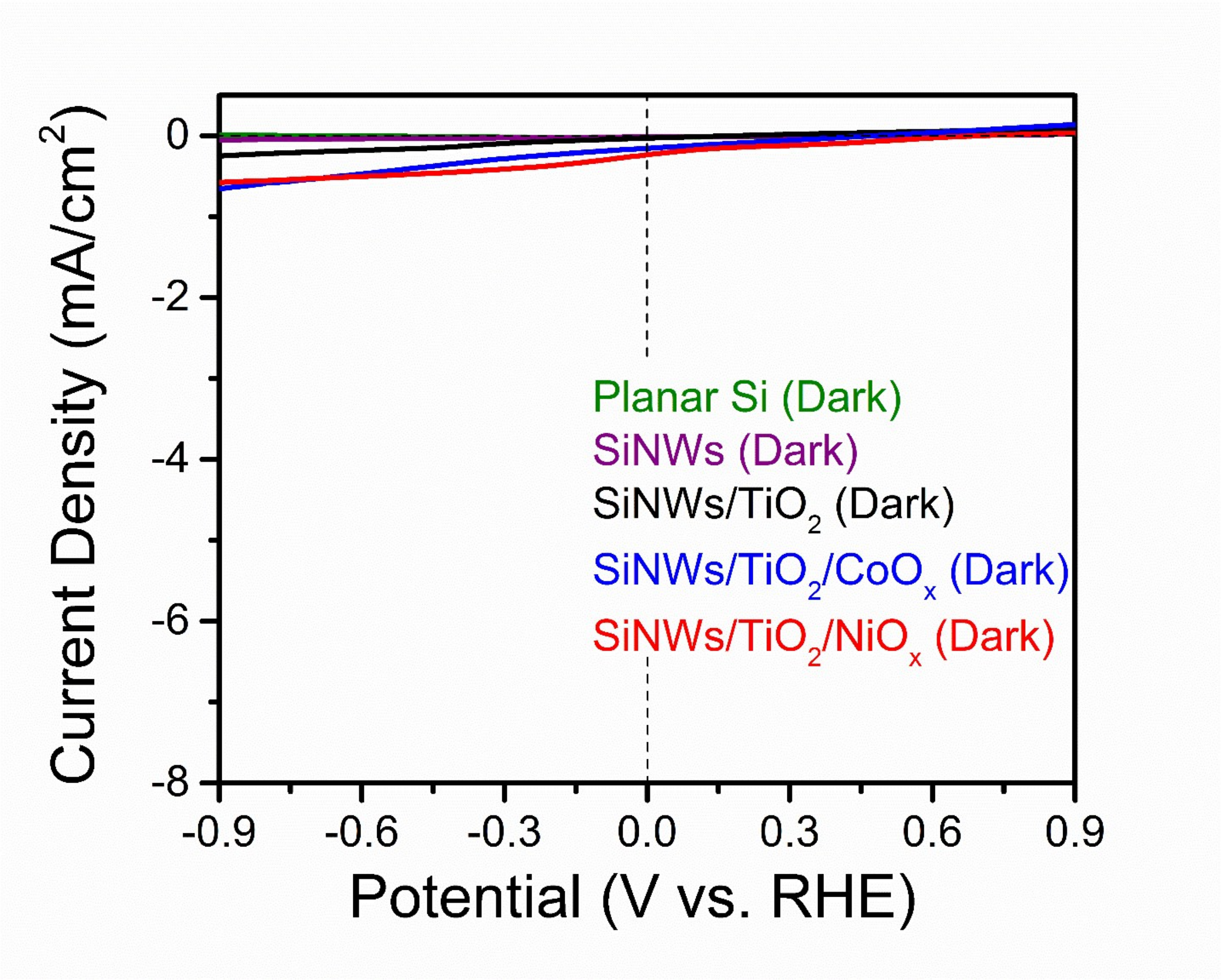

Figure S6: *:* Linear sweep voltammograms of planar p-Si, surface etched p-Si with microwires (p-Si), and functionalized p-Si photoelectrodes recorded in the dark in potassium phosphate buffer (0.2M; pH 7.00).

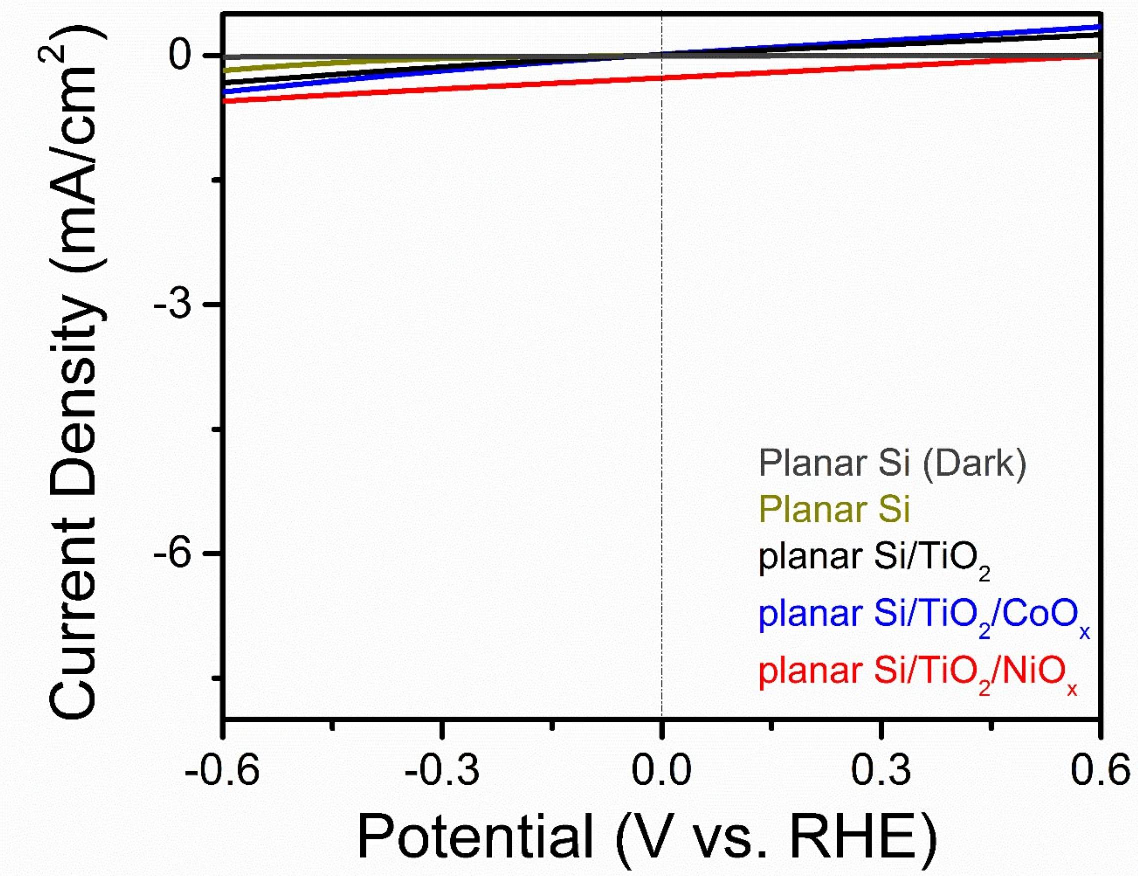

Figure S7: Linear sweep voltammograms of planar Si and functionalized planar Si measured in neutral (pH 7.0) phosphate electrolyte (0.2M KH_2PO_4+K_2HPO_4) at 1 sun illumination.

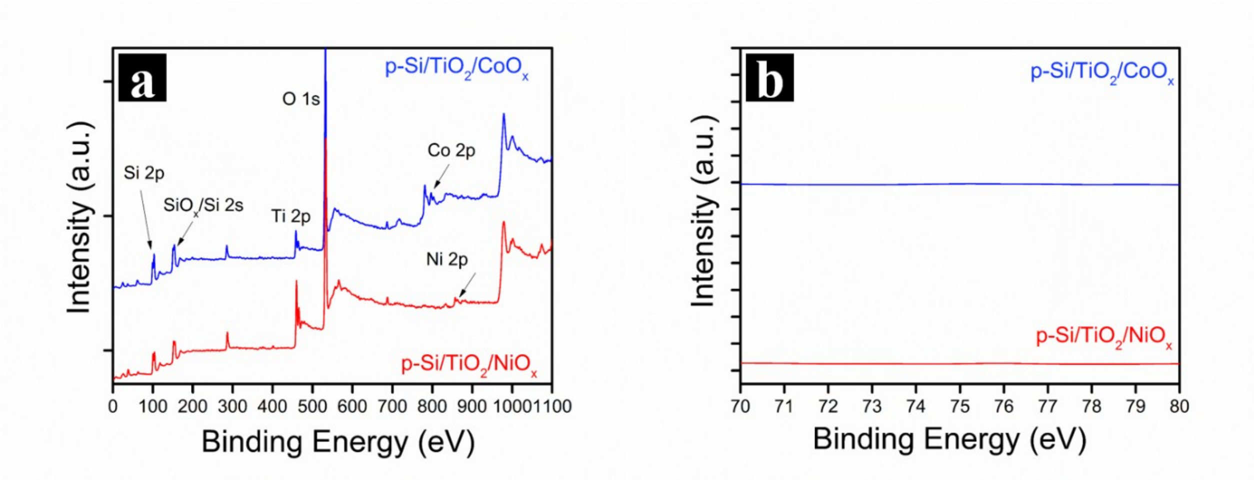

Figure S8: (a) XPS survey spectra for p-Si/TiO_2/CoO_x and p-Si/TiO_2/NiO_x acquired after the 5h stability tests. (b) extension of the energy region where Pt signals would appear: 72.7 eV (4f 7/2) and at 74.9 (4f 5/2) eV. These data indicate that Pt from the counter electrode is not deposited on the surface of the photoelectrodes.

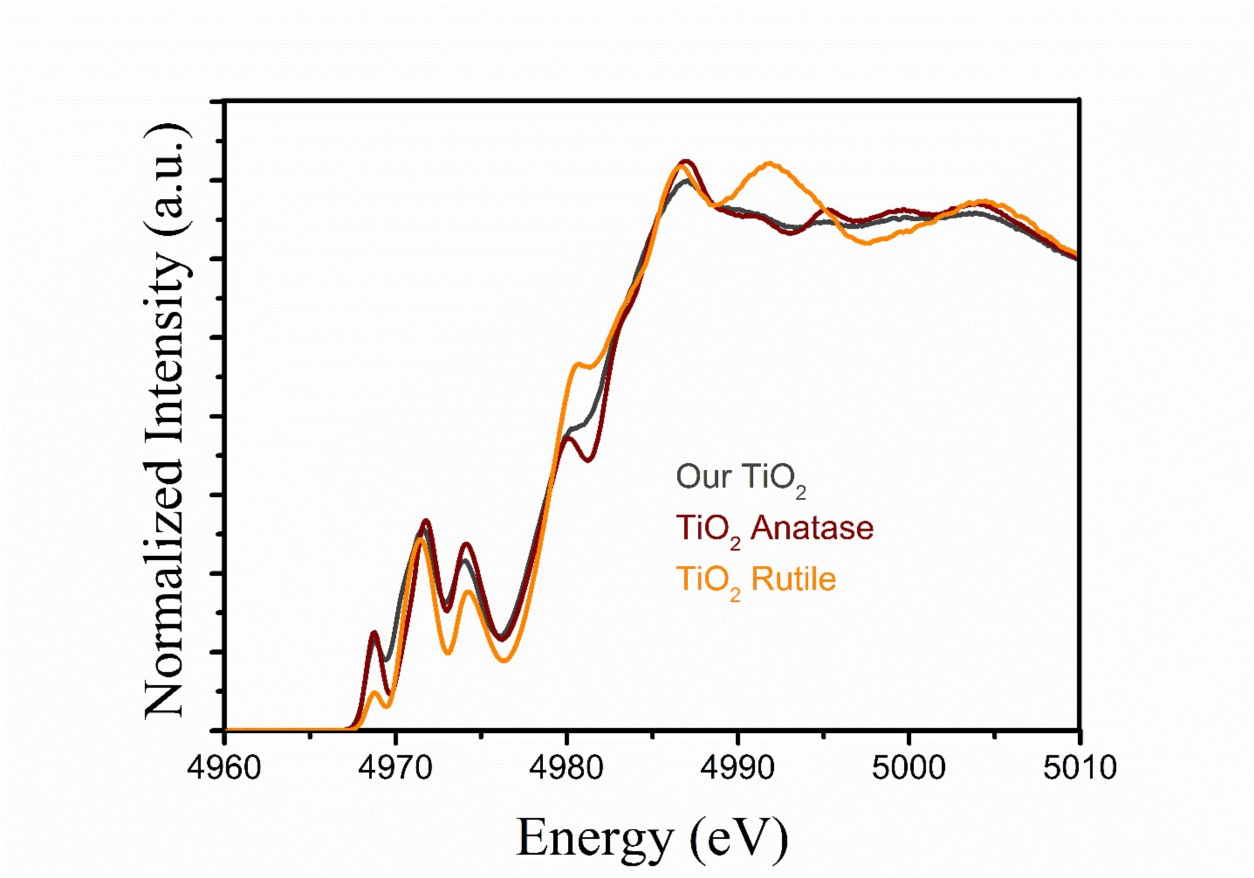

Figure S9: HERFD-XANES spectra acquired at the Ti K-edge for the reference TiO_2 anatase, TiO_2 rutile and protective TiO_2 (our).

Table S1: Photo-electrochemical performance of the functionalized p-Si photoelectrodes in different electrolytes

Substrate	**Co-Catalysts**	**Electrolyte (pH)**	**Onset Potential (V_{RHE})**	**Current Density mA/cm^2**	**Stability**	**Reference**
p-Si microwires	TiO_2/NiO_x	Phosphate buffer (7.00)	+ 0.42	> - 1.48 @ 0 V_{RHE}	>5 hours	this study
p-Si microwires	TiO_2/CoO_x	Phosphate buffer (7.00)	+ 0.27	> - 0.48 @ 0 V_{RHE}	>5 hours	this study
p-Si microwires	TiO_2/NiO_x	Artificial Seawater (8.4)	-0.12	> - 1.58 @ -0.3 V_{RHE}	>8 hours	this study
p-Si nanowires	TiO_2/Fe_2O_3	0.25 M Na_2SO_4 (7.2)	+ 0.46	- 0.55 @ 0 V_{RHE}	-	[11]
p-Si nanowires	n-ZnO	0.25 M Na_2SO_4 (7.2)	- 0.5 V Ag/AgCl	-1.45 @- 0.33 V_{RHE}	24 hours	[12]
p-Si nanowires	SnO_2/Fe_2O_3	0.25 M Na_2SO_4 (7.2)	- 0.55	~ - 1.0 @ -0.33 V_{RHE}	2.5 hours	[13]
p-Si nanowires	MoS_2	0.5 M H_2SO_4 (< 1)	+0.25	-17.6 @ 0 V_{RHE}	3 hours	[14]
p-Si nanopillars	$NiCoSe_x$	0.5 M H_2SO_4 (< 1)	+ 0.25	- 37.5 @ 0 V_{RHE}	2 hours	[15]
p-Si nanowires	Ni(TEOA)2C$_{l2}$	0.5 M H_2SO_4 (< 1)	+ 0.19	- 5.57 @-0.4V_{RHE}	24 hours	[16]
Planar Si	Ti/Ni	1 M KOH (>13)	- 0.3	-10.0 @ 0.1 V_{RHE}	12 hours	[17]
Planar Si (n^+Si)	$Ti/TiO_x/MoS_x$	1 M $HClO_4$ (<1)	0.3	-16.5 @ 0 V_{RHE}	-	[18]

Table S2: EIS fitting parameters obtained for p-Si/TiO_2, p-Si/TiO_2/CoO_x, p-Si/TiO_2/NiO_x in neutral phosphate buffer (0.2M KH_2PO_4+K_2HPO_4).

(R/Ω) **(CPE/F)**	**p-Si/TiO_2**	**p-Si/TiO_2/CoO_x**	**p-Si/TiO_2/NiO_x**
R_S	258	168	157
R_{CT1} **CPE_1**	1763 1.16×10^{-6}	1672 1.51×10^{-5}	807 4.98×10^{-5}
R_{CT2} **CPE_2**	29840 9.64×10^{-6}	6646 7.3×10^{-6}	2519 7.23×10^{-6}

References

1. K. Q. Peng, Y. J. Yan, S. P. Gao and J. Zhu, *Advanced Materials*, 2002, 14, 1164-1167.
2. J. Lyman, *J. mar. Res.*, 1940, 3, 134-140.
3. K. Chatchai, K. R. Lasanthi, R. Lars and S. Anita, *J. Environ. Manage.*, 2012, 95, S365-S368.
4. M. Rovezzi and P. Glatzel, *Semiconductor Science and Technology*, 2014, 29, 023002.
5. L. Amidani, A. Naldoni, M. Malvestuto, M. Marelli, P. Glatzel, V. Dal Santo and F. Boscherini, *Angewandte Chemie International Edition*, 2015, 54, 5413-5416.
6. P. Glatzel and U. Bergmann, *Coord. Chem. Rev.*, 2005, 249, 65-95.
7. T. Tian, J. Jiang and L. Ai, *Electro. Acta*, 2017, 224, 551-560.
8. X. Chen, D. Chen, X. Guo, R. Wang and H. Zhang, *ACS App. Mater. Inter.*, 2017, 9, 18774-18781.
9. B. Sasi and K. Gopchandran, *NanoTech.*, 2007, 18, 115613.
10. C.-Y. Lin, Y.-H. Lai, D. Mersch and E. Reisner, *Chemical Science*, 2012, 3, 3482-3487.
11. A. Kargar, J. Khamwannah, C. H. Liu, N. Park, D. Wang, S. A. Dayeh and S. Jin, *Nano energy*, 2016, 19, 289-296.
12. A. Kargar, K. Sun, Y. Jing, C. Choi, H. Jeong, Y. Zhou, K. Madsen, P. Naughton, S. Jin and G. Y. Jung, *Nano Lett.*, 2013, 13, 3017-3022.
13. A. Kargar, S. J. Kim, P. Allameh, C. Choi, N. Park, H. Jeong, Y. Pak, G. Y. Jung, X. Pan and D. Wang, *Adv. Funct. Mater.*, 2015, 25, 2609-2615.
14. Q. Ding, F. Meng, C. R. English, M. Cabán-Acevedo, M. J. Shearer, D. Liang, A. S. Daniel, R. J. Hamers and S. Jin, *J. Am. Chem. Soc.*, 2014, 136, 8504-8507.
15. H. Zhang, Q. Ding, D. He, H. Liu, W. Liu, Z. Li, B. Yang, X. Zhang, L. Lei and S. Jin, *Energy Environ. Sci.*, 2016, 9, 3113-3119.
16. W. Zhou, F. Niu, S. S. Mao and S. Shen, *App. Cat. B Enviro.*, 2018, 220, 362-366.
17. J. Feng, M. Gong, M. J. Kenney, J. Z. Wu, B. Zhang, Y. Li and H. Dai, *Nano Research*, 2015, 8, 1577-1583.
18. B. Seger, A. B. Laursen, P. C. Vesborg, T. Pedersen, O. Hansen, S. Dahl and I. Chorkendorff, *Angewandte Chemie International Edition*, 2012, 51, 9128-9131.